https://doi.org/10.5194/egusphere-2026-3945
Preprint. Discussion started: 14 July 2026

Temporal variability of air–sea carbon dioxide exchange in the coastal water of the Baltic Sea

Aki Vähä[1], Joachim Jansen[1], Kurt Spence[2], Joanna Norkko[2], Alf Norkko[2], and Ivan Mammarella[1]

[1]Institute of Atmospheric and Earth System Research/Physics, Faculty of Science, University of Helsinki, Helsinki, Finland
[2]Tvärminne Zoological Station, University of Helsinki, Hanko, Finland

Correspondence: Aki Vähä (aki.vaha@helsinki.fi)

Abstract.

Coasts are globally identified as major sinks of carbon. Still, the carbon balance in the coastal Baltic Sea remains unsolved. We analysed almost three years of continuous eddy covariance measurements of carbon dioxide fluxes in the coastal zone of the northern Baltic Sea in 2022–2024. Our results show that this coastal site acted as a small source of carbon dioxide into the atmosphere. The gap-filled carbon balances for 2023 and 2024 were 24.3 ± 0.3 g C m^{-2} and 19.2 ± 0.3 g C m^{-2}, respectively. These results are comparable with earlier results by eddy covariance in the Baltic Sea. The measurements also reveal a consistent seasonal pattern of fluxes among the years, where the sea acts as a sink of carbon dioxide in April–May, as a variable source and sink in June–September, and a source in October–March. Maximum rates of monthly uptake were measured in April and the maximum emission values in November. Data gaps were filled using a random forest model which identified wind speed and sea salinity as the most important environmental co-variates of the carbon dioxide flux. Additionally, it was shown that the non-gapfilled monthly and yearly sums are offset due to lack of night-time data and thus uneven diurnal data coverage and that gap-filling is essential in calculating the yearly balances of fluxes.

1 Introduction

The coastal ocean is globally a major sink of carbon dioxide ($\mathrm{CO_2}$) entering the marine environment from atmospheric, terrestrial, riverine and estuarine sources. Despite only covering only 7 % of total ocean area, shelf- and marginal seas (excluding estuaries and tidal wetlands) absorb 150–300 Tg C yr^{-1} of $\mathrm{CO_2}$ from the atmosphere, about 9–18 % of the total oceanic $\mathrm{CO_2}$ sink (Chau et al., 2022; Regnier et al., 2022; Dai et al., 2022), and offset 2–3 % of global anthropogenic fossil fuel emissions in 2014–2023 (Friedlingstein et al., 2025). Carbon uptake and storage in productive coastal ecosystems has been proposed as a nature-based solution to mitigate climate warming (Macreadie et al., 2021). However, estimating coastal ‘blue carbon’ budgets remains a challenge (Kuwae and Hori, 2019). This is in large part due to variability in atmospheric carbon gas fluxes over time and across diverse near-shore habitats, such as bare sand, kelp forests and eelgrass meadows. Estimating ‘blue carbon’ budgets

https://doi.org/10.5194/egusphere-2026-3945
Preprint. Discussion started: 14 July 2026

therefore relies on in-situ observations that capture spatiotemporal variability of atmospheric CO_2 fluxes in local habitats. In this study we focus on the Baltic Sea, which exhibits strong seasonality in its carbon cycle driven in part by distinct succession in its ecosystem components (e.g., Lammerant et al., 2024; Uth et al., 2024), with major implications for carbon cycling (e.g., Attard et al., 2019; Roth et al., 2023).

The Baltic Sea is a shallow brackish sea with a mean depth of 53 m and a surface area of 4.17×10^5 km^2 (Jakobsson et al., 2019). The carbon budget is dominated by riverine inputs of terrestrial organic carbon, the vast majority of which is exported to the North Sea (Kuliński and Pempkowiak, 2011). Order-of-magnitude smaller quantities of carbon are buried in sediments and exchanged with the atmosphere (Kuliński and Pempkowiak, 2011). It remains unclear whether the Baltic Sea is a net source or sink of atmospheric carbon; different upscaling methods, observation periods and locations have yielded contradictory results (Gustafsson et al., 2014). The latest integral mass balance study (Kuliński and Pempkowiak, 2011) suggests that the Baltic as a whole is a net source of carbon (1.1 ± 1.7 Tg C yr^{-1}), but more recent model-based estimates indicate that it is a net sink (-1.8 to -0.3 Tg C yr^{-1}) (Norman et al., 2013b; Gustafsson et al., 2014; Lansø et al., 2015). The assessment of the carbon budget is complicated by the strong and poorly characterized spatiotemporal variability of CO_2 fluxes. Ship-borne measurements of CO_2 partial pressure ($p$$CO_2$) or alkalinity and pH, conducted primarily in open water, suggest that the northern Bothnian Bay is a net source of carbon to the atmosphere (Algesten et al., 2006; Löffler et al., 2012), while the more productive Baltic Proper, Gulf of Riga and Gulf of Finland further south may either be net sinks (Ohlson and Anderson, 1990; Thomas and Schneider, 1999; Schneider et al., 2014) or sources (Wesslander et al., 2010). Across these regions, carbon dioxide fluxes exhibit a clear seasonality, with uptake during the spring algal bloom and emission in autumn (Thomas and Schneider, 1999; Rutgersson et al., 2008; Löffler et al., 2012; Norman et al., 2013b; Honkanen et al., 2024). Specifically, existing carbon budgets remain biased by a lack of temporally resolved observations in highly complex, diverse, and dynamic near-shore areas (Kuliński et al., 2022; Geilfus et al., 2026).

The uncertain sign of the overall atmospheric carbon flux from the Baltic Sea stems in part from poor quantification of uptake and emission events occurring at timescales of days to months. Blooms of diatoms and dinoflagellates form during several weeks in March and April when both light and nitrogen become available after ice-off (Lips et al., 2014), and can account for a major part of the annual CO_2 uptake (Honkanen et al., 2021, 2024). However, ship-based snapshots show that areas dominated by riverine inflows can be substantial CO_2 emission hotspots, even in spring (Asmala and Scheinin, 2024; Lainela et al., 2024). Upwelling of cool, CO_2-rich deep water occurs in most coastal areas of the Baltic Sea from May to September and is driven by Ekman transport under steady winds parallel to the shore (Bychkova et al., 1988; Lehmann et al., 2012; Zhang et al., 2022). Excess CO_2 persists over days–weeks (Jacobs et al., 2021) and carbon emissions associated with upwelling have, where measured, offset annual carbon uptake by 20–25 % (Kuss et al., 2006; Norman et al., 2013a). Due to a lack of high-frequency monitoring, the importance of uptake and emission events for the annual carbon budget remains unclear.

Year-round monitoring is also required to assess how climate change alters carbon uptake and emission processes in the Baltic Sea. For example, in the near-shore Finnish archipelago, a ship-based campaign showed a rapid drop in $p$$CO_2$ during a storm following a heatwave in the autumn of 2018 (Humborg et al., 2019), suggesting that rapid degassing of accumulated CO_2 could be a major source of carbon to the atmosphere. At the same time, year-round eddy covariance (EC) flux measurements

https://doi.org/10.5194/egusphere-2026-3945
Preprint. Discussion started: 14 July 2026

at Utö, further offshore, indicated that 2018 had the lowest annual net CO_2 emissions out of five years, as the exceptionally high summer temperatures promoted cyanobacterial growth (Honkanen et al., 2024). Climate warming increases the frequency of ice-free years and atmospheric heatwaves in the Baltic region (Meier et al., 2022) but assessing their impact on 'blue carbon' uptake requires continuous observations. EC flux measurements allow direct, automated and high-frequency estimates of air–sea carbon and energy exchange, but only two EC flux towers in the Baltic region have collected long-term flux data: Östergarnsholm near Gotland, Sweden (1995–present) (Rutgersson et al., 2008, 2020) and Utö in the Gulf of Finland (2017–2021) (Honkanen et al., 2021), both over relatively deep coastal shelves (water depth 10–50 m in tower footprint).

We currently lack continuous carbon flux observations in shallow (water depth < 5 m) near-shore environments. Vegetated shallow regions of the Baltic Sea are home to key habitats for blue carbon storage, such as eelgrass meadows, and act as a biogeochemical filter for nutrients and organic matter from land to the open sea (Asmala et al., 2017; Carstensen et al., 2020). Consequently, they are increasingly recognized as important sites for carbon production, exchange, and burial (Humborg et al., 2019; Kuliński et al., 2022; Roth et al., 2023). However, carbon budgets for the Baltic have been based on sediment burial rates, which exclude water column metabolism and transport processes (Tokoro et al., 2019; Roth et al., 2023), or model estimates, which vary considerably depending on underlying geospatial data and assumptions about driving processes (Lansø et al., 2015). Net annual carbon fluxes in shallow vegetated areas may be similar to those offshore, because algal blooms, driving carbon uptake, occur across depth zones (Lips et al., 2014), but this is yet unknown. This limits our ability to accurately estimate carbon fluxes based on measurements of $p\mathrm{CO}_2$, water temperature and wind speed, for example, from ships of opportunity.

In this study, we present almost three years of EC observations of CO_2 fluxes from a shallow coastal area at Tvärminne Zoological Station (TZS) in the southern Finnish archipelago. We examine the annual cycles of these fluxes and compare them to those of deeper and more exposed coastal waters at Östergarnsholm and Utö. Using random-forest-based gap-filling, we estimate monthly and annual net carbon exchange. Our dataset addresses the gap in carbon flux data that currently exists for very shallow, vegetated coastal areas in the Baltic Sea, and complements past and ongoing carbon flux monitoring offshore.

2 Materials and methods

2.1 Site description

The eddy covariance tower is located on the western end of an islet (Idgrund) on the Baltic Sea coast in southern Finland at 59.842° N, 23.250° E (Fig. 1, Fig. S1). The islet is approximately 15 m $\times$ 25 m in size and 2 m at its highest point. The location is a semi-enclosed bay in the vicinity of the Tvärminne Zoological Station of the University of Helsinki. The site contributes to the Integrated Carbon Observation System (ICOS) as an associated ecosystem station (FI-Tvm). In addition, the EC setup is part of an integrated Station for Measuring Ecosystem-Atmosphere Relations (SMEAR) site run by the University of Helsinki (Thakur et al., 2025) and part of Centre for Coastal Ecosystem and Climate Change Research (CoastClim, https://www.coastclim.org/, most recent access 17 April 2026).

The over-water fetch around the tower measures between 100 m and 800 m, except for the sectors in the south-south-east and south-west where it is approximately 1–3 km. The bay borders the mainland in the west and north and open water with

https://doi.org/10.5194/egusphere-2026-3945
Preprint. Discussion started: 14 July 2026

islands in other directions. The sea surrounding the EC tower is mostly 4–8 m deep, but shallower areas exist close to the land. The seafloor consists of bare soft-sediment and hard substrate areas, as well as vegetated habitats (see e.g. Lammerant et al., 2024). The seabed sediments in the immediate vicinity of the site are primarily medium sands with interspersed areas of silty deposits. To the southwest of the tower, the aquatic vegetation is dominated by eelgrass (*Zostera marina*), and to the north and southeast by brown algae (*Fucus vesiculosus*). Annual algal blooms typically occur in April–May (dinoflagellates and diatoms) and August (cyanobacteria) (Uth et al., 2024).

The sea surface temperature at the measurement site varies annually between 0 °C and approximately 20 °C and the annual mean is 9 °C. An increasing trend in water temperature has been observed (Goebeler et al., 2022; Stockmayer and Lehmann, 2023). The water is brackish with a salinity of 5–7 PSU (Merkouriadi and Leppäranta, 2014). Sea ice occurs almost every winter at the site, although the duration of the ice cover may vary between 0 and 3 months. Similarly, ice thickness and area fraction are highly variable. There are no long-term ice phenology observations at the EC site. Air temperature and precipitation are measured by the Finnish Meteorological Institute's (FMI) permanent weather station 300 m from the EC site on the mainland. The mean annual air temperature and mean annual precipitation during the reference period 1991–2020 were 6.5 °C and 634 mm, respectively.

The geology of the area is characterized by granodiorite bedrock and the maximum elevation is 10–25 m above sea level. Both the mainland and larger islands are covered in forest with Scots pine (*Pinus sylvestris*) and European alder (*Alnus glutinosa*) as the dominant species, but there are numerous areas of non-vegetated bedrock surface, especially on the small islands in southeast and southwest. Although no major urban or agricultural areas are located near the site, river discharge from the northeast delivers organic carbon and nutrients from inland catchments to the study area.

2.2 Eddy covariance and ancillary measurement setup

The EC tower stands atop a concrete base which protects the mast from rafting sea ice. The measurement height is 4.2 m above the mean sea level. The height from the actual sea surface may vary by approximately 0.5 m from the mean due to sea level changes (Fig. S2). These are caused by wind forcing and the total water budget of the Baltic Sea such that the highest water levels occur during westerly or south-westerly winds, and typically during late autumn and winter. Tides are negligible at the site.

The three Cartesian wind speed components u, v and w and the sonic temperature T_s are measured by a uSonic-3 Scientific sonic anemometer (METEK GmbH., Elmshorn, Germany), installed at the top of a 3 m tall mast (Vaisala Oyj., Vantaa, Finland). The gas analyser is a LI-7200RS (LI-COR Biosciences Inc., Lincoln, Nebraska, USA) for measuring CO_2 and H_2O dry mole fractions. Measurements with the sonic anemometer commenced on 18 February 2022 and CO_2 flux measurements on 10 March 2022. The time interval used for the data analysis in this work is 10 March 2022 – 31 December 2024.

The LI-7200RS's air intake tube is a standard, insulated intake tube (LI-COR). It is 1 m in length and has an inner diameter of 5 mm. The flow speed is kept at a constant 12 L/min. The instrument itself is mounted on the EC mast but the flow unit and field computers are placed in cabinets 15 m away from the mast. Electric cables from the EC mast to the cabinets run along an

https://doi.org/10.5194/egusphere-2026-3945
Preprint. Discussion started: 14 July 2026

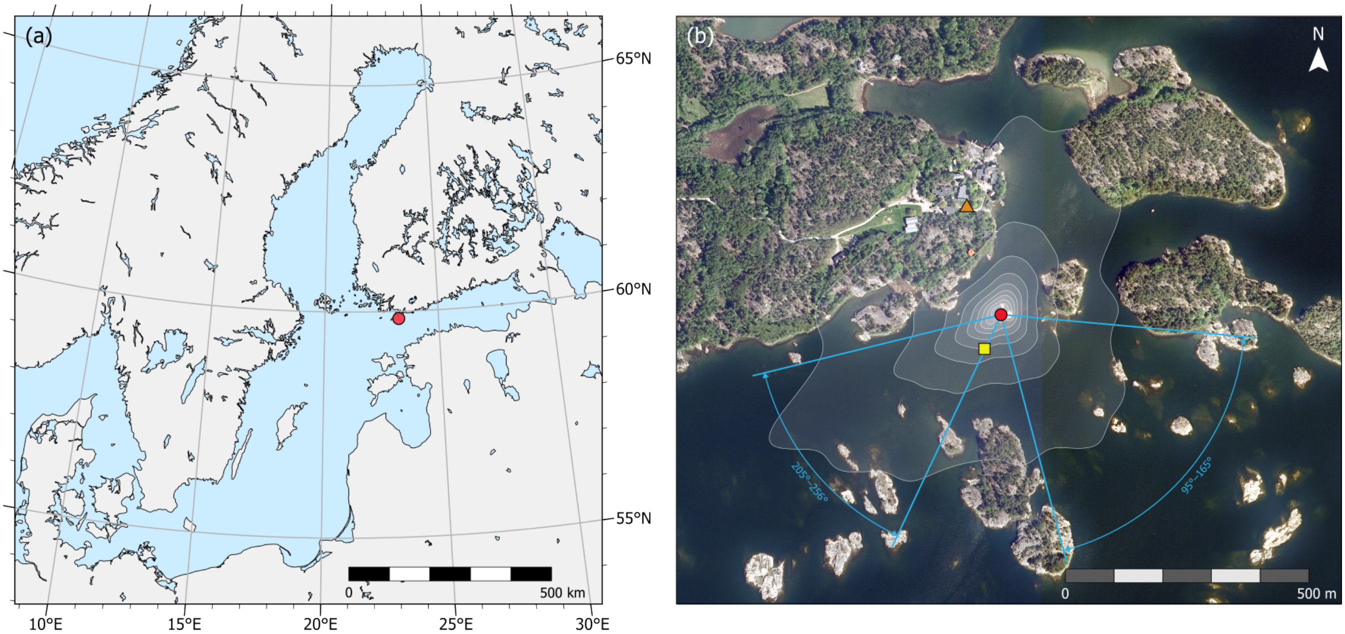

Figure 1. (a) Map of the Baltic Sea and its surroundings and the location of the EC site (red circle). (b) Flux footprint climatology and the two wind sectors used in our analysis. The grey lines and the shading represent the area within which flux signals have accumulated. The lines are at 10 % increments and the outermost line represents the 90 % flux footprint climatology. The blue lines mark the sectors from which the fluxes were accepted. Fluxes from outside these sectors were potentially influenced by land and discarded. The red circle denotes the EC site. The yellow square marks the location of the Monicoast buoy and the orange triangle the location of the FMI weather station.

elevated wire 1 m above the ground and sea to prevent damage from moving sea ice. The cables are heated in order to avoid ice buildup.

Air temperature and relative humidity are measured with a HMP155 probe (Vaisala Oyj., Vantaa, Finland) on the islet at a height of 4 m above mean sea level. Water temperature and salinity are measured approximately 100 m south from the EC tower at a depth of 3.5 m using a YSI Exo2 sonde (Xylem Inc., Yellow Springs, Ohio, USA) aboard the monitoring buoy 'Monicoast'. Global and reflected shortwave (SW) and incoming and outgoing longwave (LW) radiation components are measured above water on the southern side of the islet with a CNR4 net radiometer (OTT HydroMet B.V., Delft, The Netherlands). Photosynthetically active radiation (PAR) is measured with a PQS1 radiometer (OTT HydroMet B.V.).

2.3 Eddy covariance data processing

The turbulent flux of CO_2 is defined as

$$FCO_2 = \frac{\rho_\mathrm{d}}{M_\mathrm{d}}\overline{w'\chi'_{\mathrm{CO_2}}}, \tag{1}$$

https://doi.org/10.5194/egusphere-2026-3945
Preprint. Discussion started: 14 July 2026

Table 1. Coefficients for the cospectral fit grouped according to the atmospheric stability z/L and frequency n.

	a	b	c
$z/L < 0, n \leq 1$	14.7	22.0	1.6
$z/L < 0, n \geq 1$	3.7	3.8	2.3
$z/L > 0, n \leq 1$	5.8	4.9	2.1
$z/L > 0, n \geq 1$	9.2	3.8	2.7

where ρ_d and M_d are the dry air density and the molar mass, respectively, and $\overline{w'\chi'_{\mathrm{CO_2}}}$ is the covariance of vertical wind speed w and the CO_2 dry mole fraction $\chi_{\mathrm{CO_2}}$ (Aubinet et al., 2000). Fluxes were calculated with the EddyUH software (Mammarella et al., 2016), and it included the following processing steps: de-spiking of time series (Mauder et al., 2013) and mean removal by block-averaging, double coordinate rotation of wind velocity components, time lag adjustment between the w and $\chi_{\mathrm{CO_2}}$ time series by maximising their cross-covariance within a predefined window, and calculation of 30 min fluxes. Fluxes were corrected for high frequency spectral losses (Mammarella et al., 2009) by dividing the fluxes by the flux attenuation factor F_a, defined as

$$\mathrm{F_a} = \frac{\int_0^\infty C_m(f) TF\, df}{\int_0^\infty C_m(f)\, df}, \tag{2}$$

where TF = $[1+(2\pi f\tau)^2]^{-1}$ is the first order transfer function with empirically derived CO_2 response time $\tau = 0.13s$, and C_m is the site specific normalized model cospectrum derived by fitting a functional form by Kaimal et al. (1972) to the wT cospectrum C_{wT},

$$C_\mathrm{m} = \frac{f C_{wT}}{\mathrm{cov}\,(uT)} = \frac{an}{(1+bn)^c}, \tag{3}$$

where f is the natural frequency, $n = zf/U$ is the dimensionless frequency, z the measurement height, U the mean wind speed and a, b and c are the fitting coefficients. The fitting was done separately for stable and unstable atmospheric conditions, defined by the stability parameter $\zeta = z/L$, where L is the Obukhov length. Table 1 reports the coefficient values for different stability classes, and Figure 2 shows one example of the average cospectra for CO_2 and T_s.

The data logging system suffered a synchronisation problem during October 2023 – June 2024. During this period, the gas analysers' internal clocks would fluctuate between -9 and $+9$ s relative to the system time. The time series were corrected by determining the shifted lag time for w and LI-7200RS CO_2 mole fraction with the cross-covariance maximisation method and with several partially overlapping windows in order to reduce scatter in the estimated lag times and then shifting the LI-7200RS time series accordingly. Average lag when the instrument was functioning correctly was 0.25 s for CO_2.

The flux footprint climatology was determined using the model by Kljun et al. (2015). The input variables were the mean wind speed, wind direction (WD), Obukhov length, standard deviation of lateral wind speed, friction velocity u_* and boundary layer height $h_\mathrm{BL} = 1000$ m (constant). The measurement height was assumed constant, i.e. sea level fluctuations were not taken into account. The calculated footprint climatology (Fig. 1b) shows that 90 % of the fluxes originate within 600 m of the

https://doi.org/10.5194/egusphere-2026-3945
Preprint. Discussion started: 14 July 2026

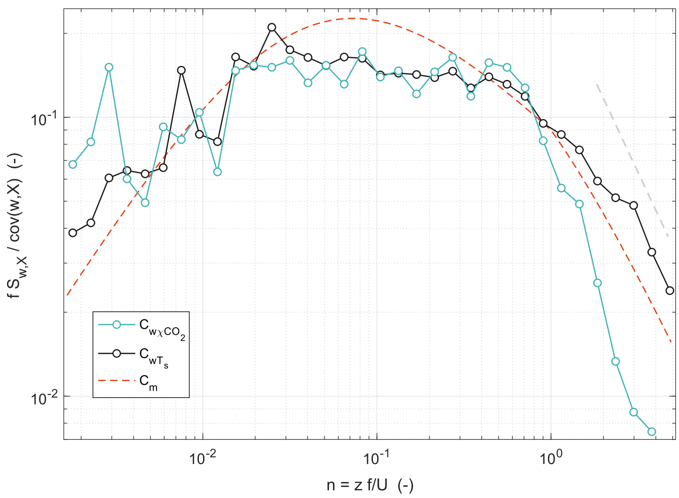

Figure 2. Averaged cospectra of sonic temperature (black) and CO_2 mixing ratio (cyan) from April 2023 as a function of the dimensionless frequency n. The spectra are multiplied by frequency f and normalised by covariances $\overline{w'\chi'_{CO_2}}$ or $\overline{w'T'_s}$. The spectra are from instances of unstable and near-neutral atmospheric stability. The dashed red line shows the cospectral model function C_m. The dashed grey line shows the expected $-4/3$ inertial subrange scaling.

tower. This allows for unobstructed trace gas flux measurements from two sectors: $95° \leq$ WD $\leq 165°$ and $205° \leq$ WD $\leq 256°$. Increasing the measurement height by 1 m would extend the upwind footprint distance by approximately 20 %. Since the available fetch in the accepted sectors exceeds 1 km in the southeast (SE) and 2 km in the southwest (SW), such a change in measurement height – resulting from variations in sea level – would not significantly affect the footprint composition or alter the accepted sectors. The small islands in the flux footprint are nonvegetated, i.e. they do not affect the trace gas flux measurements. In the nomenclature of Rutgersson et al. (2020), the accepted sectors represent Category 2, or open-water sectors where the wave field is affected by land and where source density of fluxes can be heterogeneous. The excluded sectors represent Category 3. Instances when the wind was in the accepted sectors comprised 37.3 % of the total measurement period.

The fluxes were screened using the following quality criteria: wind direction as stated above, flux stationarity test (Mahrt, 1998) with the nonstationarity ratio for $FCO_2 < 3$, gas analyser diagnostics, and requiring the 30-minute standard deviation of χ_{CO_2} to be less than 2 ppm. The criterion for the standard deviation was used to identify occasions when advection of CO_2 occurs especially during situations with a strong land–sea breeze. The criteria partly overlap each other and in total, the screening retained 22.9 % of the raw FCO_2, or 11269 data records in total (Tab. 2). The data screening was effective in removing outliers from the raw CO_2 fluxes, and the remaining fluxes were generally small in magnitude.

Monthly data coverage for FCO_2 varied between 0 % and 45 %. The fraction of quality-controlled fluxes to the total amount of data as a function of time of day varied between 0 % and 71 % (Fig. S3). Between March and August, there was a considerable difference in the amount of accepted flux data between day and night, daytime being defined as PAR > 10 μmol $m^{-2}\,s^{-1}$. In most extreme cases such as in May, August and November 2024, the fraction of accepted nocturnal data was close

https://doi.org/10.5194/egusphere-2026-3945
Preprint. Discussion started: 14 July 2026

Table 2. Quality filtering criteria for FCO_2 and the percentage of flux data they retain.

Criterion	Data retained (%)
Wind direction	37.3
Flux stationarity	78.9
σCO_2	92.6
Gas analyser diagnostics	93.2
Total	22.9

to 0 %. The primary cause for this is the land–sea breeze that occurred during many nights. There is also seasonal variability in the amount of data with the highest amount of accepted data occurring during summer.

2.4 Gap-filling

We obtained annual sums of CO_2 fluxes by gap-filling half-hourly, quality-controlled CO_2 fluxes. A random forest model (Breiman, 2001) was used because tree-based methods do not assume a specific relation between variables (i.e. exponential) and consistently outperform other gap-filling methods for eddy covariance fluxes (Irvin et al., 2021; Mahabbati et al., 2021). Fluxes were gap-filled for the continuous period between 10 March 2022 and 31 December 2024, based on availability of the independent variables. The gap-filling step was important because of a clear daytime bias in the number of half-hourly fluxes (Fig. S3), and a large fraction of missing CO_2 flux data after quality control (77.1 %). The independent variables in the model were year, day-of-year, hour, wind speed, wind direction, total incoming shortwave radiation, total incoming long-wave radiation, photosynthetically active radiation (PAR), air temperature, surface water temperature, surface water salinity, and the atmospheric CO_2 mixing ratio. Because continuous timeseries of all independent variables are required to gap-fill CO_2 fluxes, we first imputed the independent variables via iterative random forest chaining using the missRanger function in R, a fast implementation of the missForest algorithm (Stekhoven and Bühlmann, 2012). The fraction of data gaps was relatively small for the measured independent variables, ranging from 3 % (wind speed) to 21 % (salinity). We tuned the hyperparameter for the number of variables randomly sampled as candidates at each split using TuneMtryFast in the TuneRanger package in R (Probst et al., 2019). Finally, we fitted the random forest model using the ranger function in R with 1500 trees (Wright and Ziegler, 2017) and predicted values for each missing CO_2 flux estimate. The out-of-bag coefficient of determination (R^2), or variance explained by the model, was 0.51.

The random forest model can be used to identify the most important drivers of the CO_2 flux. We used standardized permutation importance scores, which reflect the reduction in model performance upon shuffling the values of each predictor. In the gap-filling model described above, the most important predictor variables were wind speed, day-of-year and salinity (Fig. 3). However, strong collinearity of predictors (e.g. surface water and air temperature) reduces the importance scores of both, which can bias predictor ranking. We therefore repeated the random forest analysis without air temperature and PAR, such that the absolute value of Kendall's τ was larger than 0.7 for each predictor pair (Dormann et al., 2013). In the second model, the most important predictors were still wind speed, day-of-year and salinity.

https://doi.org/10.5194/egusphere-2026-3945
Preprint. Discussion started: 14 July 2026

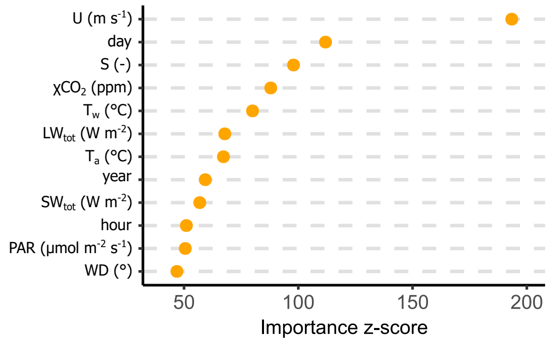

Figure 3. Variable importance of CO_2 flux random forest predictor.

2.5 Estimates of flux uncertainty

The uncertainty $\delta_{F,i}$ of each half-hourly flux measurement was estimated as the random error with the method of Finkelstein and Sims (2001). The uncertainty estimates were heteroscedastic with their magnitude depending on the magnitude of the fluxes. The method of Lenschow et al. (2000) was used to estimate the instrumental error. Its mean magnitude was only 18 % of the total random uncertainty of $F\mathrm{CO_2}$. It can be concluded that the random uncertainty of the $\mathrm{CO_2}$ fluxes was mainly caused by the stochastic nature of the turbulence itself and not by the instrumentation. For the error estimation of the gap-filled fluxes, a linear dependence on the absolute magnitude of the flux was used, calculated from the measured fluxes: $\delta_{F,i} = 0.287\,|F_i| + 0.05$ $\mathrm{\mu mol\,m^{-2}\,s^{-1}}$.

The propagation of uncertainty was estimated with two different methods. When calculating means of fluxes for time-of-day bins, the uncertainty estimates $\delta_{F,i}$ for individual flux values F_i were treated as independent and identically distributed, in which case the total uncertainty of flux ensemble mean $\langle F \rangle$ with N observations could be calculated with a quadratic propagation of uncertainty: $\Delta_{\langle F \rangle} = \sqrt{\sum_{i=1}^{N} (\delta_{F,i})^2 / N^2}$ (Rannik et al., 2016). For the aggregated monthly and yearly sums and weekly means of gap-filled fluxes, we applied a Monte Carlo method following Richardson and Hollinger (2007). In this approach, new realizations of the flux time series were generated by replacing each individual flux value F_i with $F_i + \epsilon_{F,i}$, where $\epsilon_{F,i}$ was randomly drawn from a Laplace distribution with the estimated flux random uncertainty $\delta_{F,i}$ as the scale parameter. A total of $N_{\mathrm{MC}} = 10000$ of these realisations were computed and their corresponding aggregates (sum or mean) were evaluated. The resulting distribution of the aggregated fluxes is approximately Gaussian, its mean converges to the aggregate of the original gap-filled flux time series and the spread, expressed as the 95 % confidence interval, gives an estimate for the total uncertainty. These uncertainty estimates were calculated separately for all weekly means, as well as monthly and yearly sums.

https://doi.org/10.5194/egusphere-2026-3945
Preprint. Discussion started: 14 July 2026

3 Results

3.1 Meteorological and environmental conditions

The meteorological and environmental conditions during 2022–2024 are shown in Fig.4 and Fig. S2. The air temperature at the EC site varied between -18 °C in January 2024 and $+26$ °C in June 2022, showing a clear seasonal pattern where the highest temperatures are observed during June–August and the lowest during December–March. The annual mean air temperatures at the FMI weather station were $+7.3$ °C in 2022, $+6.7$ °C in 2023 and $+7.7$ °C in 2024 which all exceeded the 30-year mean of $+6.5$ °C. Winter temperatures exhibited the largest interannual variability, winter 2023–24 having the coldest temperatures of the measurement period. During other seasons, the interannual variability was smaller.

The water temperature followed the air temperature, but with smaller and delayed variability. The maximum water temperature was $+22.6$ °C which occurred in June 2022 and the minimum -0.4 °C in January 2023. The largest differences in water temperature between years occurred in May–August. During this time, the temperature varied between $+6$ °C and $+22.6$ °C. The temperatures in autumn, winter, and spring were fairly consistent throughout the three years. Photosynthetically active radiation (PAR) followed a consistent yearly pattern, modified by cloudiness, with maximum in the summer and minimum in winter. The sea surface salinity varied between 4.6 and 7.2 PSU and did not show any seasonal pattern (Fig. S2d). Sea ice occurred sporadically during the winter 2022–2023 and from early January to early March 2024, although with some intermittent periods of ice breakups.

Wind speeds were generally the highest during autumn and winter but the overall seasonal differences were small. The wind was largely channeled between land areas and southwesterly wind over the main open-water sector prevailed (Fig. S4). The highest 30-minute mean wind speed up to 18 $\mathrm{m\ s^{-1}}$ was observed in the SW sector. A notable land–sea breeze in the land sectors 0°–90° and 270°–360° was apparent especially in spring and summer during low synoptic activity (Fig. S5).

3.2 CO_2 fluxes

Time series of F_{CO_2} are presented in Fig.5. Individual 30-minute values had relatively large scatter but were mainly small with absolute magnitudes of less than 1 $\mathrm{\mu mol\ m^{-2}\ s^{-1}}$ for 99 % of the fluxes. Monthly means of F_{CO_2} varied between -0.30 $\mathrm{\mu mol\ m^{-2}\ s^{-1}}$ and $+0.44$ $\mathrm{\mu mol\ m^{-2}\ s^{-1}}$. The weekly means varied between -0.48 $\mathrm{\mu mol\ m^{-2}\ s^{-1}}$ and $+0.60$ $\mathrm{\mu mol\ m^{-2}\ s^{-1}}$. The mean uncertainty of the measured 30-minute FCO_2 was 0.12 ± 0.15 $\mathrm{\mu mol\ m^{-2}\ s^{-1}}$ (mean and standard deviation).

The distribution of gap-filled FCO_2 has a small positive offset compared to that of non-gapfilled values, visible as the small difference in the weekly means (Fig. 5). In addition, the distribution of the gap-filled values tends towards zero more than their non-gapfilled respective counterparts. The weekly means of gap-filled FCO_2 varied between -0.2 and $+0.3$ $\mathrm{\mu mol\ m^{-2}\ s^{-1}}$ whereas the non-gapfilled weekly means had larger variability, the flux varying between -0.5 and $+0.7$ $\mathrm{\mu mol\ m^{-2}\ s^{-1}}$.

Comparing the mean monthly gap-filled FCO_2 with the non-gapfilled monthly means reveals a difference in the non-gapfilled monthly means (Fig. 6). The difference was positive when the gap-filled monthly balance was more than approximately 0.1 $\mathrm{\mu mol\ m^{-2}\ s^{-1}}$. This holds primarily for months where the diurnal distribution of accepted FCO_2 was approximately uniform, that is, in September–February. The same difference is reflected in the annual sums where the non-gapfilled

https://doi.org/10.5194/egusphere-2026-3945
Preprint. Discussion started: 14 July 2026

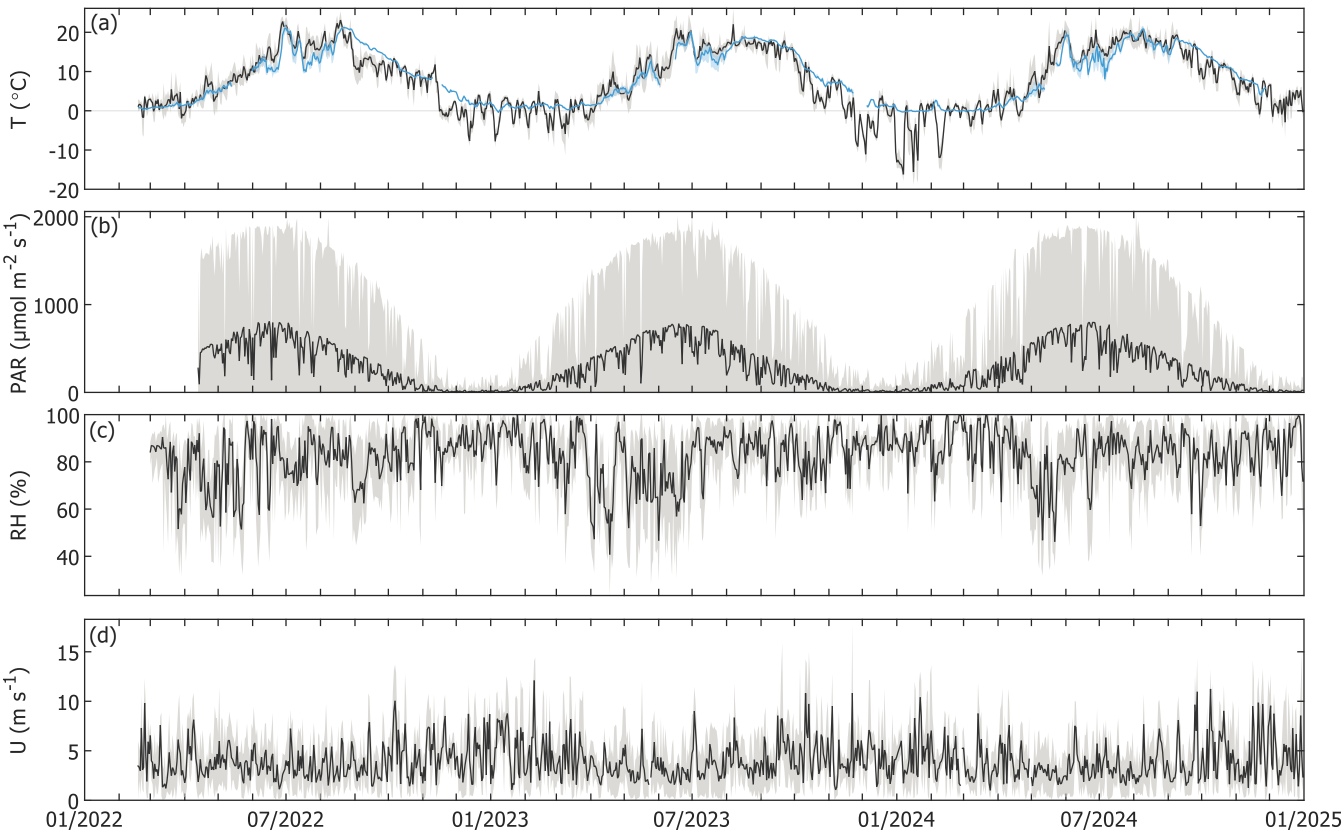

Figure 4. Meteorological and environmental conditions at the Tvärminne EC site FI-Tvm during 2022–2024. The line and the shading denote the daily mean and maximal daily variability, respectively. (a) Air (black) and water (blue) temperature (T). (b) Photosynthetically active radiation (PAR). (c) Relative humidity (RH). (d) Wind speed (U) at 4.2 m above the mean sea level.

Table 3. Annual sums of the quality-controlled non-gapfilled and gap-filled FCO_2 in g C m^{-2} and their estimated uncertainties. The year 2022 starts from 10 March and is therefore presented in brackets.

	2022	2023	2024
Not gap-filled	(-1.6 ± 1.9)	13.3 ± 5.9	-10.7 ± 2.1
Gap-filled	(16.5 ± 0.5)	24.3 ± 0.5	19.2 ± 0.4

https://doi.org/10.5194/egusphere-2026-3945
Preprint. Discussion started: 14 July 2026

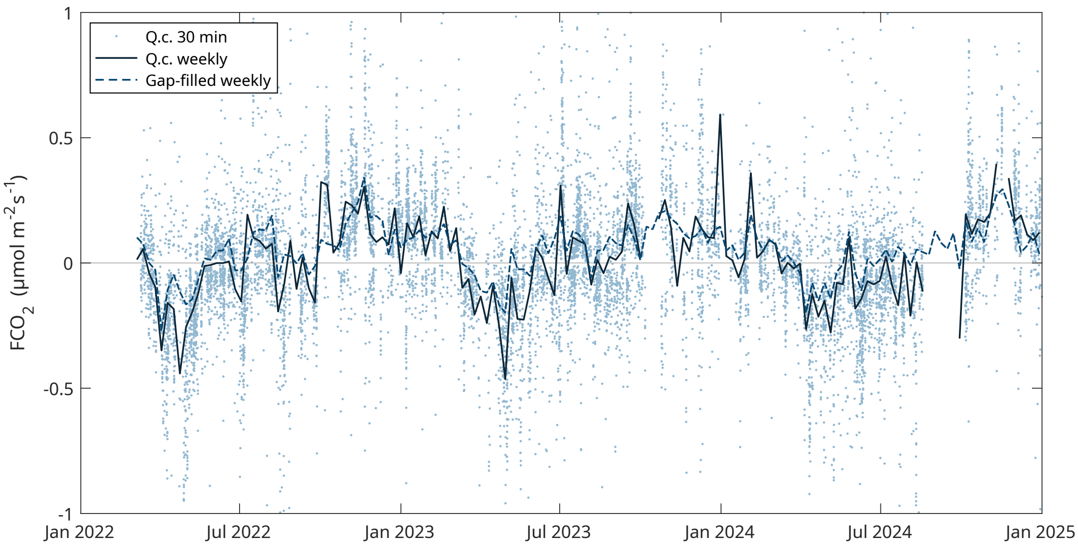

Figure 5. Time series of the 30-minute FCO_2 (dots), weekly means of the quality-controlled fluxes (solid line), and weekly means of gap-filled FCO_2 (dashed line). Positive values indicate an upward flux, i.e. surface emission.

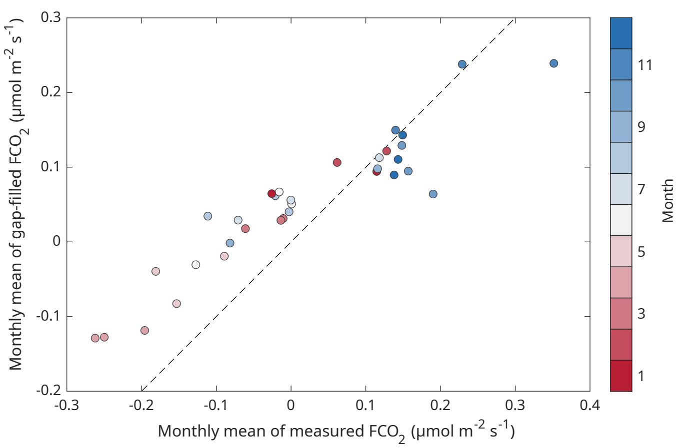

Figure 6. Monthly means of measured versus gap-filled FCO_2. The colours indicate the month. The dashed line shows the 1:1 relation.

https://doi.org/10.5194/egusphere-2026-3945
Preprint. Discussion started: 14 July 2026

sums skew more negative by 11–30 $\mathrm{gC\ m^{-2}}$. Additionally, it can be seen that the gap-filled and non-gapfilled monthly means do not match except in only a few cases. The underlying reason for these differences is the non-uniform diurnal distribution of fluxes where the majority of gaps occur in the nighttime.

3.3 Diurnal, seasonal and interannual variability of CO_2 fluxes

CO_2 fluxes exhibited a clear diurnal cycle. Statistically significant differences between day and night $F\mathrm{CO_2}$ (2-sided t test, $p < 0.05$) were found mainly between April and October (Tab. S1). The diel cycle of fluxes was visible as a U shape in April–August, most prominently in April and May (Fig. 7). Fluxes during daytime became negative in March and remained so until August–September. Nighttime fluxes were approximately 0 $\mathrm{\mu mol\ m^{-2}\ s^{-1}}$ or slightly positive (0.1–0.2 $\mathrm{\mu mol\ m^{-2}\ s^{-1}}$) in December–March. In April and May, the nighttime fluxes stayed mostly negative apart from a few nighttime hours of positive fluxes. In June–November, the nighttime fluxes were between 0 and 0.6 $\mathrm{\mu mol\ m^{-2}\ s^{-1}}$. The largest daytime sink, approximately -0.4 $\mathrm{\mu mol\ m^{-2}\ s^{-1}}$, occurred in April, whereas the greatest emissions occurred in October–November with flux values of approximately 0.6 $\mathrm{\mu mol\ m^{-2}\ s^{-1}}$.

The CO_2 fluxes had consistent seasonal patterns that become apparent when averaging the 30-minute fluxes over several days or weeks (Fig. 8). In mid or late March, the sea turned into a carbon sink. Peak uptake of CO_2 occurred in late April, with weekly means between -0.2 and -0.4 $\mathrm{\mu mol\ m^{-2}\ s^{-1}}$. Over May–September, the sea was approximately at a net zero CO_2 exchange but there was both intra- and interannual variability in the fluxes. The sea became a source of CO_2 typically in September, albeit the onset of this stage varied from year to year, and this stage lasted until the beginning of the next spring. Weekly means during this stage were approximately between 0 and $+0.4$ $\mathrm{\mu mol\ m^{-2}\ s^{-1}}$. In 2022 and 2023, the spring uptake was stronger than in 2024, but on the other hand, the daytime uptake of CO_2 was stronger in 2024 and lasted until September. Maximum monthly emissions occurred consistently in November with weekly mean CO_2 emissions reaching $+0.4$ $\mathrm{\mu mol\ m^{-2}\ s^{-1}}$. The interannual variability of monthly fluxes was at lowest in February–April whereas the highest variability was observed in June–November. Especially during September–November, there were changes in $F\mathrm{CO_2}$ over timescales of a few days.

Yearly balances of non-gapfilled and gap-filled $F\mathrm{CO_2}$ are presented in Table 3. The gap-filled balances are positive, indicating that the footprint area was a carbon source to the atmosphere, and the balances show interannual variability. All the gap-filled balances are larger than their respective non-gap-filled balances by 11–30 g C $\mathrm{m^{-2}}$. We note that the non-gapfilled balances show approximately a net zero total carbon exchange during 2022–2024. With this amount of gaps and the uneven diurnal distribution of data, gap-filling is essential in resolving the total balance.

4 Discussion

4.1 Temporal variability of CO_2 fluxes

The CO_2 fluxes measured at the Tvärminne EC site exhibit a clear and recurring temporal structure across multiple timescales. Seasonally, three distinct phases can be identified: (i) a spring uptake period from late March to mid-May, (ii) a transition

https://doi.org/10.5194/egusphere-2026-3945
Preprint. Discussion started: 14 July 2026

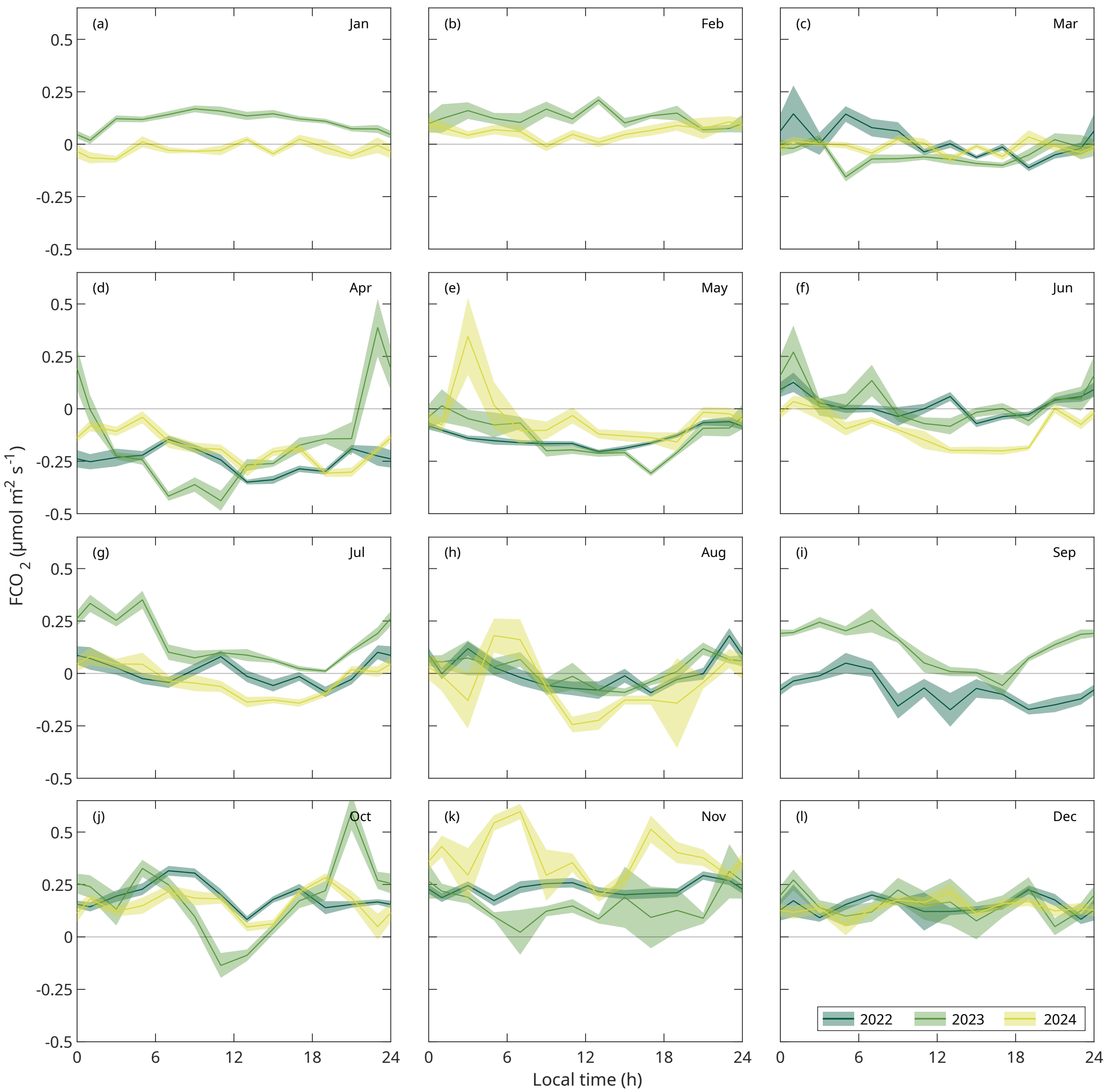

Figure 7. Diurnal patterns of FCO_2 in different months (subplots) and years (colours of lines). The fluxes are averages into 2 h bins. The line and the shaded area show the mean and the estimated uncertainty for each bin.

https://doi.org/10.5194/egusphere-2026-3945
Preprint. Discussion started: 14 July 2026

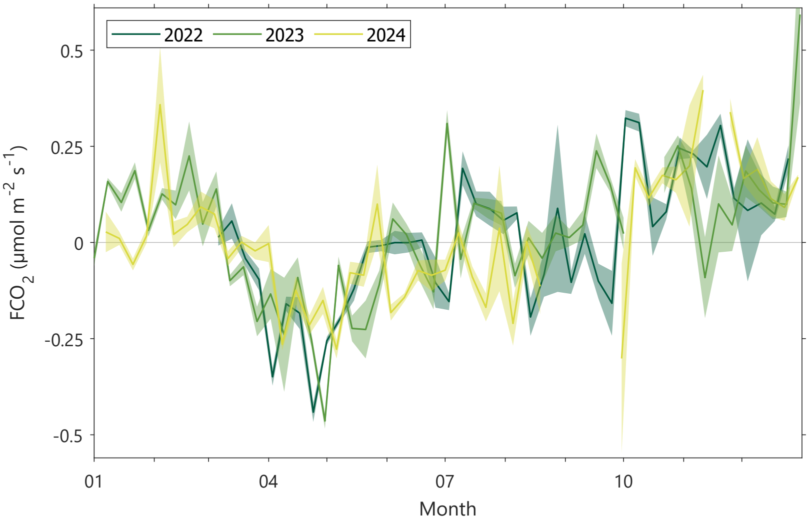

Figure 8. Weekly means of CO_2 fluxes with the individual years drawn on top of each other. The shaded area shows the uncertainty estimate, obtained by the Monte Carlo method.

period with alternating uptake and emission from late spring to early autumn, and (iii) a period dominated by emissions during late autumn and winter. This seasonal cycle is consistent across years but is modulated by considerable interannual variability, particularly during the latter half of the year. Superimposed on the seasonal signal is a pronounced diurnal cycle, characterised by daytime CO_2 uptake and nighttime emission or near-zero flux. These diel dynamics indicate rapid changes in the balance between production and respiration processes within the system.

The magnitude of the observed fluxes is comparable to those reported for other mid- and high-latitude coastal and estuarine systems (Dai et al., 2022). In addition, the temporal patterns observed at Tvärminne broadly resemble those reported at the two other long-term EC sites in the Baltic Sea, Östergarnsholm (Gutiérrez-Loza et al., 2022) and Utö (Honkanen et al., 2024), although important differences emerge when examined in more detail.

The onset of the spring CO_2 uptake at Tvärminne occurs at approximately the same time as at Utö, suggesting a regionally coherent trigger for the spring uptake. However, differences become more evident during summer. At Tvärminne, the system acts as a weaker and more variable CO_2 sink than at Utö, particularly during June–July, with CO_2 fluxes of approximately 0 or slightly negative. Compared to Östergarnsholm, the spring uptake at Tvärminne begins slightly later but reaches a larger magnitude and for a longer duration. During summer, the fluxes at Tvärminne are similar in magnitude to those at Östergarnsholm; however, after June, monthly mean fluxes at Tvärminne turn positive, whereas they generally remain negative at Utö and Östergarnsholm until August.

Spring uptake in Tvärminne starting later than in Östergarnsholm but reaching a similar magnitude could indicate the role of benthic macrophytes in the system. Indeed, previous aquatic eddy covariance measurements in the area have shown that benthic carbon fluxes can exceed air–sea fluxes by an order of magnitude in certain habitats (Attard et al., 2019), highlighting

https://doi.org/10.5194/egusphere-2026-3945
Preprint. Discussion started: 14 July 2026

the importance of shallow-water macrophyte systems. In particular, *Fucus vesiculosus*-dominated habitats exhibit high gross primary production and act as strong carbon sinks. Benthic processes also contribute year-round: production increases rapidly with light in late winter, while wintertime gross primary production (22–30 %) and respiration (27–31 %) constitute a substantial fraction of annual totals. Although the exact footprint-weighted contributions of different benthic habitats remain uncertain, their combined influence is likely a key factor shaping the observed temporal variability in CO_2 fluxes at Tvärminne.

During autumn and early winter, all three sites act as CO_2 sources, but emissions are typically smaller at Tvärminne. A likely contributing factor is seasonal sea ice, which reduces air–sea gas exchange. At Tvärminne, fluxes approached zero during periods of ice cover in winter 2023–2024, whereas Utö and Östergarnsholm experienced little or no ice during 2022–2024. Although this suggests that ice cover may partly explain inter-site differences, more accurate observations are required to confirm this mechanism.

Despite differences in seasonal dynamics, all three sites act as net annual CO_2 sources. Annual carbon balances at Tvärminne (24.3 and 19.2 g C m^{-2} for 2023 and 2024, respectively) are remarkably similar in magnitude to those reported for Utö (27.1 g C m^{-2}) and Östergarnsholm (approximately 25 g C m^{-2}, not gap-filled), even though these latter sites are more representative of open-sea conditions.

4.2 Drivers of CO_2 fluxes

The CO_2 flux is governed by two primary controls: the turbulence in the water-side surface layer, which regulates the magnitude of the flux, and the air–sea CO_2 gradient, which determines its sign. Our random forest model identified wind speed as the most important predictor of CO_2 flux. Wind-driven turbulence is widely recognised as the dominant control on air–sea gas exchange (Upstill-Goddard, 2006) and operates on the same temporal scale as flux variability. In the absence of direct $p\mathrm{CO_2}$ measurements, identifying other specific drivers is challenging; however, the observed flux variability can be interpreted in the context of known $p\mathrm{CO_2}$ dynamics in the Baltic Sea.

Surface water $p\mathrm{CO_2}$ in the Baltic Sea exhibits strong spatial and temporal variability (Bittig et al., 2024). This variability is influenced by physical processes such as riverine input, upwelling, frontal dynamics, and vertical mixing (Lainela et al., 2024), as well as by biological activity of pelagic (Uth et al., 2024) and benthic (Rohlfer et al., 2026) components. The Tvärminne site is located in a transitional zone between CO_2-rich inner estuaries and the typically CO_2-depleted open Baltic Sea during summer, making it particularly sensitive to both physical and biological drivers (Asmala and Scheinin, 2024).

On seasonal timescales, the balance between biological production and respiration is the dominant control on $p\mathrm{CO_2}$ and thus on CO_2 flux (Gutiérrez-Loza et al., 2021). The minimum of $p\mathrm{CO_2}$ usually occurs during the spring phytoplankton bloom and again in late summer during cyanobacterial blooms (BACC II Author Team, 2015). These patterns are consistent with our observations at Tvärminne, where maximum CO_2 uptake occurred in spring, followed by secondary uptake periods during summer.

The spring phytoplankton bloom is primarily driven by radiation and limited by nitrogen availability (Neumann et al., 2012). The consistent timing of spring uptake over the three years observed in our data supports this mechanism. Similarly, benthic uptake initiation has been shown to be radiation-controlled (Attard et al., 2019). Cyanobacterial blooms in late summer are

https://doi.org/10.5194/egusphere-2026-3945
Preprint. Discussion started: 14 July 2026

temperature-dependent and limited by sulfur availability (Kahru et al., 2020), and are more sensitive to climatic and environmental variability than spring blooms (Beltran-Perez and Waniek, 2022). The observed variability in summertime fluxes at our site is consistent with these findings and with reported variability in summer phytoplankton communities (Uth et al., 2024).

The observed diurnal changes in CO_2 flux, including sign reversals, imply corresponding diurnal cycles in $p CO_2$. Attard et al. (2019) demonstrated that aquatic gross primary production exhibits diurnal variation, accompanied by sign changes in O_2 flux, indicating alternating CO_2 super- and subsaturation. In Utö, Honkanen et al. (2021) observed diurnal $p CO_2$ cycles from April to October, with maxima in the morning and minima in the afternoon. The largest diurnal amplitudes ($\sim$100 ppm) occurred in August. These cycles are primarily driven by biological activity (photosynthesis and respiration), although mixing processes can occasionally dominate. Similar conclusions regarding the roles of air–sea exchange and advection have been reported elsewhere in the Baltic Sea (e.g., Wesslander et al., 2011; Lansø et al., 2017). These dynamics are consistent with our observed flux behaviour.

In a recent study, Geilfus et al. (2026) confirmed that biological activity modifies $p CO_2$ in the archipelago surrounding our study site and that the magnitude of the modification is greater for sheltered and semi-sheltered locations. Apart from the biological factors, the variability in surface water $p CO_2$ was strongly associated with salinity gradients, suggesting that riverine input is a major source of dissolved inorganic and organic carbon.

Our random forest model identified wind speed, day of year, and sea surface salinity as the most important predictors of CO_2 flux. Wind-driven turbulence is widely recognised as the dominant control on air–sea gas exchange (Upstill-Goddard, 2006) and operates on the same temporal scale as flux variability. Salinity acts as a proxy for water mass characteristics, including dissolved gas concentrations. For example, Humborg et al. (2019) and Geilfus et al. (2026) have showed that $p CO_2$ in the Tvärminne region closely follows salinity gradients. Despite the clear role of biological processes in driving flux variability in shallow coastal waters, net shortwave radiation was not a major predictor in our model. This likely reflects lag effects: radiation influences the rate of change of $p CO_2$ rather than its instantaneous value, and therefore does not peak simultaneously with $p CO_2$ or CO_2 flux. Instead, the day-of-year variable effectively captures the seasonal cycle of ecosystem metabolism.

5 Conclusions

We report results from almost three years of eddy covariance measurements on the coast of the northern Baltic Sea. This coastal site was found to be a source of CO_2 into the atmosphere, similar in magnitude as two other long-term EC stations on the central or northern Baltic Sea. This result was obtained through gap-filling. In the annual patterns of the CO_2 fluxes, we identified three major features: a sink period in April–May, a variable sink and source period in June–September and a source period in October–March. Mean diurnal flux patterns show a difference in day- and nighttime fluxes and a daytime sink of CO_2 from April to August. Comparison with literature reveals a similar pattern of fluxes measured elsewhere around the Baltic Sea. Overall, CO_2 flux variability at Tvärminne arises from the interplay of physical transport processes, biological production and respiration, and air–sea exchange dynamics, operating across diel to seasonal timescales.

https://doi.org/10.5194/egusphere-2026-3945
Preprint. Discussion started: 14 July 2026

Data availability. Eddy covariance, radiation and flux ancillary data (ICOS ETC L2 ARCHIVE) are available at the ICOS Carbon portal, DOI: 10.18160/S6HM-CP8Q (Mammarella et al., 2025). The complete dataset used in this work is available at https://doi.org/10.5281/zenodo.21135816 (Vähä et al., 2026).

Author contributions. IM and JJ conceptualized and supervised the study. AN, JN and IM acquired funding. AV, KS and IM conducted the EC measurements. AV processed the EC data and performed the analysis. JJ carried out the random forest analysis. AV, JJ and IM prepared the first draft of the manuscript. All authors reviewed the manuscript.

Competing interests. The authors declare that they have no competing interests.

Acknowledgements. AV acknowledges funding from the Onni Talas Foundation.

EU Horizon Europe-Framework Programme for Research and Innovation (Grant No. 101056921-GreenFeedBack and LiweFor No. 101079192) and ICOS-FI via funding from the University of Helsinki.

This study utilized research infrastructure facilities at Tvärminne Zoological Station, University of Helsinki, as part of FINMARI (Finnish Marine Research Infrastructure consortium). The authors want to thank the scientific and technical staff of the station for their assistance. This is a publication from the Center for Coastal Ecosystem and Climate Change Research (CoastClim).

The authors want to thank Timo Vesala for his comments on the Discussion.

Fig. 1b contains data from the Finnish Land Survey's Topographical database by the license CC-BY-4.0.

Meteorological observations from the Finnish Meteorological Institute are used under the license CC-BY-4.0.

https://doi.org/10.5194/egusphere-2026-3945
Preprint. Discussion started: 14 July 2026

References

Algesten, G., Brydsten, L., Jonsson, P., Kortelainen, P., Löfgren, S., Rahm, L., Räike, A., Sobek, S., Tranvik, L., Wikner, J., and Jansson, M.: Organic carbon budget for the Gulf of Bothnia, Journal of Marine Systems, 63, 155–161, https://doi.org/10.1016/j.jmarsys.2006.06.004, 2006.

Asmala, E. and Scheinin, M.: Persistent hot spots of CO_2 and CH_4 in coastal nearshore environments, Limnology and Oceanography Letters, 9, 119–127, https://doi.org/10.1002/lol2.10370, 2024.

Asmala, E., Carstensen, J., Conley, D. J., Slomp, C. P., Stadmark, J., and Voss, M.: Efficiency of the coastal filter: Nitrogen and phosphorus removal in the Baltic Sea, Limnology and Oceanography, 62, S222–S238, https://doi.org/10.1002/lno.10644, 2017.

Attard, K. M., Rodil, I. F., Glud, R. N., Berg, P., Norkko, J., and Norkko, A.: Seasonal ecosystem metabolism across shallow benthic habitats measured by aquatic eddy covariance, Limnology and Oceanography Letters, 4, 79–86, https://doi.org/10.1002/lol2.10107, 2019.

Aubinet, M., Vesala, T., and Papale, D., eds.: Eddy covariance: a practical guide to measurement and data analysis, Springer, Dordrecht, the Netherlands, 2000.

BACC II Author Team, ed.: Second Assessment of Climate Change for the Baltic Sea Basin, Regional Climate Studies, Springer, Cham, Switzerland, https://doi.org/10.1007/978-3-319-16006-1, 2015.

Beltran-Perez, O. D. and Waniek, J. J.: Inter-annual variability of spring and summer blooms in the eastern Baltic Sea, Frontiers in Marine Science, 9, https://doi.org/10.3389/fmars.2022.928633, 2022.

Bittig, H. C., Jacobs, E., Neumann, T., and Rehder, G.: A regional $p\mathrm{CO_2}$ climatology of the Baltic Sea from in situ $p\mathrm{CO_2}$ observations and a model-based extrapolation approach, Earth System Science Data, 16, 753–773, https://doi.org/10.5194/essd-16-753-2024, 2024.

Breiman, L.: Random forests, Machine Learning, 45, 5–32, https://doi.org/10.1023/A:1010933404324, 2001.

Bychkova, A. I., Viktorov, S. V., and Shumakher, D. A.: A relationship between the large-scale atmospheric circulation and the origin of coastal upwelling in the Baltic, Meteorol. Gidrol., 10, 91–98, 1988.

Carstensen, J., Conley, D. J., Almroth-Rosell, E., Asmala, E., Bonsdorff, E., Fleming-Lehtinen, V., Gustafsson, B. G., Gustafsson, C., Heiskanen, A.-S., Janas, U., Norkko, A., Slomp, C., Villnäs, A., Voss, M., and Zilius, M.: Factors regulating the coastal nutrient filter in the Baltic Sea, AMBIO, 49, 1194–1210, https://doi.org/10.1007/s13280-019-01282-y, 2020.

Chau, T. T. T., Gehlen, M., and Chevallier, F.: A seamless ensemble-based reconstruction of surface ocean $p\mathrm{CO_2}$ and air-sea CO_2 fluxes over the global coastal and open oceans, Biogeosciences, 19, 1087–1109, https://doi.org/10.5194/bg-19-1087-2022, 2022.

Dai, M., Su, J., Zhao, Y., Hofmann, E. E., Cao, Z., Cai, W.-J., Gan, J., Lacroix, F., Laruelle, G. G., Meng, F., Müller, J. D., Regnier, P. A. G., Wang, G., and Wang, Z.: Carbon fluxes in the coastal ocean: synthesis, boundary processes, and future trends, Annual Review of Earth and Planetary Sciences, 50, 593–626, https://doi.org/10.1146/annurev-earth-032320-090746, 2022.

Dormann, C. F., Elith, J., Bacher, S., Buchmann, C., Carl, G., Carré, G., Marquéz, J. R. G., Gruber, B., Lafourcade, B., Leitão, P. J., Münkemüller, T., McClean, C., Osborne, P. E., Reineking, B., Schröder, B., Skidmore, A. K., Zurell, D., and Lautenbach, S.: Collinearity: a review of methods to deal with it and a simulation study evaluating their performance, Ecography, 36, 27–46, https://doi.org/https://doi.org/10.1111/j.1600-0587.2012.07348.x, 2013.

Finkelstein, P. and Sims, P.: Sampling error in eddy correlation flux measurements, Journal of Geophysical Research: Atmospheres, 106, 3503–3509, https://doi.org/10.1029/2000JD900731, 2001.

Friedlingstein, P., O'Sullivan, M., Jones, M. W., Andrew, R. M., Hauck, J., Landschützer, P., Le Quéré, C., Li, H., Luijkx, I. T., Olsen, A., Peters, G. P., Peters, W., Pongratz, J., Schwingshackl, C., Sitch, S., Canadell, J. G., Ciais, P., Jackson, R. B., Alin, S. R., Arneth, A., Arora, V., Bates, N. R., Becker, M., Bellouin, N., Berghoff, C. F., Bittig, H. C., Bopp, L., Cadule, P., Campbell, K., Chamberlain, M. A., Chandra, N., Chevallier, F., Chini, L. P., Colligan, T., Decayeux, J., Djeutchouang, L. M., Dou, X., Duran Rojas, C., Enyo, K., Evans, W., Fay, A. R., Feely, R. A., Ford, D. J., Foster, A., Gasser, T., Gehlen, M., Gkritzalis, T., Grassi, G., Gregor, L., Gruber, N., Gürses, O., Harris, I., Hefner, M., Heinke, J., Hurtt, G. C., Iida, Y., Ilyina, T., Jacobson, A. R., Jain, A. K., Jarníková, T., Jersild, A., Jiang, F., Jin, Z., Kato, E., Keeling, R. F., Klein Goldewijk, K., Knauer, J., Korsbakken, J. I., Lan, X., Lauvset, S. K., Lefèvre, N., Liu, Z., Liu, J., Ma, L., Maksyutov, S., Marland, G., Mayot, N., McGuire, P. C., Metzl, N., Monacci, N. M., Morgan, E. J., Nakaoka, S.-I., Neill, C., Niwa, Y., Nützel, T., Olivier, L., Ono, T., Palmer, P. I., Pierrot, D., Qin, Z., Resplandy, L., Roobaert, A., Rosan, T. M., Rödenbeck, C., Schwinger, J., Smallman, T. L., Smith, S. M., Sospedra-Alfonso, R., Steinhoff, T., Sun, Q., Sutton, A. J., Séférian, R., Takao, S., Tatebe, H., Tian, H., Tilbrook, B., Torres, O., Tourigny, E., Tsujino, H., Tubiello, F., van der Werf, G., Wanninkhof, R., Wang, X., Yang, D., Yang, X., Yu, Z., Yuan, W., Yue, X., Zaehle, S., Zeng, N., and Zeng, J.: Global Carbon Budget 2024, Earth System Science Data, 17, 965–1039, https://doi.org/10.5194/essd-17-965-2025, 2025.

Geilfus, N.-X., Delille, B., Villnäs, A., and Norkko, A.: Spatial heterogeneity of GHG dynamics across an estuarine ecosystem, Biogeosciences, 23, 1931–1948, https://doi.org/10.5194/bg-23-1931-2026, 2026.

Goebeler, N., Norkko, A., and Norkko, J.: Ninety years of coastal monitoring reveals baseline and extreme ocean temperatures are increasing off the Finnish coast, Communications Earth & Environment, 3, 215, https://doi.org/10.1038/s43247-022-00545-z, 2022.

Gustafsson, E., Deutsch, B., Gustafsson, B. G., Humborg, C., and Mörth, C.-M.: Carbon cycling in the Baltic Sea — The fate of allochthonous organic carbon and its impact on air–sea CO_2 exchange, Journal of Marine Systems, 129, 289–302, https://doi.org/10.1016/j.jmarsys.2013.07.005, 2014.

Gutiérrez-Loza, L., Wallin, M. B., Sahlée, E., Holding, T., Shutler, J. D., Rehder, G., and Rutgersson, A.: Air–sea CO_2 exchange in the Baltic Sea—A sensitivity analysis of the gas transfer velocity, Journal of Marine Systems, 222, 103 603, https://doi.org/10.1016/j.jmarsys.2021.103603, 2021.

Gutiérrez-Loza, L., Nilsson, E., Wallin, M. B., Sahlée, E., and Rutgersson, A.: On physical mechanisms enhancing air–sea CO_2 exchange, Biogeosciences, 19, 5645–5665, https://doi.org/10.5194/bg-19-5645-2022, 2022.

Honkanen, M., Müller, J. D., Seppälä, J., Rehder, G., Kielosto, S., Ylöstalo, P., Mäkelä, T., Hatakka, J., and Laakso, L.: The diurnal cycle of pCO$_2$ in the coastal region of the Baltic Sea, Ocean Science, 17, 1657–1675, https://doi.org/10.5194/os-17-1657-2021, 2021.

Honkanen, M., Aurela, M., Hatakka, J., Haraguchi, L., Kielosto, S., Mäkelä, T., Seppälä, J., Siiriä, S.-M., Stenbäck, K., Tuovinen, J.-P., Ylöstalo, P., and Laakso, L.: Interannual and seasonal variability of the air–sea CO_2 exchange at Utö in the coastal region of the Baltic Sea, Biogeosciences, 21, 4341–4359, https://doi.org/10.5194/bg-21-4341-2024, 2024.

Humborg, C., Geibel, M. C., Sun, X., McCrackin, M., Mörth, C.-M., Stranne, C., Jakobsson, M., Gustafsson, B., Sokolov, A., Norkko, A., and Norkko, J.: High emissions of carbon dioxide and methane from the coastal Baltic Sea at the end of a summer heat wave, Frontiers in Marine Science, 6, 493, https://doi.org/10.3389/fmars.2019.00493, 2019.

Irvin, J., Zhou, S., McNicol, G., Lu, F., Liu, V., Fluet-Chouinard, E., Ouyang, Z., Knox, S. H., Lucas-Moffat, A., Trotta, C., Papale, D., Vitale, D., Mammarella, I., Alekseychik, P., Aurela, M., Avati, A., Baldocchi, D., Bansal, S., Bohrer, G., Campbell, I, D., Chen, J., Chu, H., Dalmagro, H. J., Delwiche, K. B., Desai, A. R., Euskirchen, E., Feron, S., Goeckede, M., Heimann, M., Helbig, M., Helfter, C., Hemes, K. S., Hirano, T., Iwata, H., Jurasinski, G., Kalhori, A., Kondrich, A., Lai, D. Y. F., Lohila, A., Malhotra, A., Merbold, L., Mitra, B., Ng, A., Nilsson, M. B., Noormets, A., Peichl, M., Rey-Sanchez, A. C., Richardson, A. D., Runkle, B. R. K., Schafer, K. V. R., Sonnentag, O., Stuart-Haentjens, E., Sturtevant, C., Ueyama, M., Valach, A. C., Vargas, R., Vourlitis, G. L., Ward, E. J., Wong, G. X., Zona, D., Alberto, M. C. R., Billesbach, D. P., Celis, G., Dolman, H., Friborg, T., Fuchs, K., Gogo, S., Gondwe, M. J., Goodrich, J. P., Gottschalk, P., Hortnagl, L., Jacotot, A., Koebsch, F., Kasak, K., Maier, R., Morin, T. H., Nemitz, E., Oechel, W. C., Oikawa, P. Y., Ono, K., Sachs, T., Sakabe, A., Schuur, E. A., Shortt, R., Sullivan, R. C., Szutu, D. J., Tuittila, E.-S., Varlagin, A., Verfaillie, J. G., Wille, C., Windham-Myers, L., Poulter, B., and Jackson, R. B.: Gap-filling eddy covariance methane fluxes: Comparison of machine learning model predictions and uncertainties at FLUXNET-CH4 wetlands, Agricultural and Forest Meteorology, 308, https://doi.org/10.1016/j.agrformet.2021.108528, 2021.

Jacobs, E., Bittig, H. C., Gräwe, U., Graves, C. A., Glockzin, M., Müller, J. D., Schneider, B., and Rehder, G.: Upwelling-induced trace gas dynamics in the Baltic Sea inferred from 8 years of autonomous measurements on a ship of opportunity, Biogeosciences, 18, 2679–2709, https://doi.org/10.5194/bg-18-2679-2021, 2021.

Jakobsson, M., Stranne, C., O'Regan, M., Greenwood, S. L., Gustafsson, B., Humborg, C., and Weidner, E.: Bathymetric properties of the Baltic Sea, Ocean Science, 15, 905–924, https://doi.org/10.5194/os-15-905-2019, 2019.

Kahru, M., Elmgren, R., Kaiser, J., Wasmund, N., and Savchuk, O.: Cyanobacterial blooms in the Baltic Sea: Correlations with environmental factors, Harmful Algae, 92, https://doi.org/10.1016/j.hal.2019.101739, 2020.

Kaimal, J. C., Wyngaard, J. C., Izumi, Y., and Coté, O. R.: Spectral characteristics of surface-layer turbulence, Quarterly Journal of the Royal Meteorological Society, 98, 563–589, https://doi.org/https://doi.org/10.1002/qj.49709841707, 1972.

Kljun, N., Calanca, P., Rotach, M. W., and Schmid, H. P.: A simple two-dimensional parameterisation for Flux Footprint Prediction (FFP), Geoscientific Model Development, 8, 3695–3713, https://doi.org/10.5194/gmd-8-3695-2015, 2015.

Kuliński, K. and Pempkowiak, J.: The carbon budget of the Baltic Sea, Biogeosciences, 8, 3219–3230, https://doi.org/10.5194/bg-8-3219-2011, 2011.

Kuliński, K., Rehder, G., Asmala, E., Bartosova, A., Carstensen, J., Gustafsson, B., Hall, P. O. J., Humborg, C., Jilbert, T., Jürgens, K., Meier, H. E. M., Müller-Karulis, B., Naumann, M., Olesen, J. E., Savchuk, O., Schramm, A., Slomp, C. P., Sofiev, M., Sobek, A., Szymczycha, B., and Undeman, E.: Biogeochemical functioning of the Baltic Sea, Earth System Dynamics, 13, 633–685, https://doi.org/10.5194/esd-13-633-2022, 2022.

Kuss, J., Roeder, W., Wlost, K.-P., and DeGrandpre, M. D.: Time-series of surface water CO_2 and oxygen measurements on a platform in the central Arkona Sea (Baltic Sea): seasonality of uptake and release, Marine Chemistry, 101, 220–232, https://doi.org/10.1016/j.marchem.2006.03.004, 2006.

Kuwae, T. and Hori, M., eds.: Blue Carbon in Shallow Coastal Ecosystems, Springer Singapore, Singapore, 1 edn., https://doi.org/10.1007/978-981-13-1295-3, 2019.

Lainela, S., Jacobs, E., Luik, S.-T., Rehder, G., and Lips, U.: Seasonal dynamics and regional distribution patterns of CO_2 and CH_4 in the north-eastern Baltic Sea, Biogeosciences, 21, 4495–4519, https://doi.org/10.5194/bg-21-4495-2024, 2024.

Lammerant, R., Rohlfer, E. K., Norkko, A., and Gustafsson, C.: Seasonality strongly affects short-term C-storage in coastal macrophyte communities, Limnology and Oceanography, 69, 700–711, https://doi.org/10.1002/lno.12524, 2024.

Lansø, A., Sørensen, L., Christensen, J., Rutgersson, A., , and Geels, C.: The influence of short-term variability in surface water $p\mathrm{CO_2}$ on modelled air–sea CO_2 exchange, Tellus B, 69, 1302 670, https://doi.org/10.1080/16000889.2017.1302670, 2017.

Lansø, A. S., Bendtsen, J., Christensen, J. H., Sørensen, L. L., Chen, H., Meijer, H. A. J., and Geels, C.: Sensitivity of the air-sea CO_2 exchange in the Baltic Sea and Danish inner waters to atmospheric short-term variability, Biogeosciences, 12, 2753–2772, https://doi.org/10.5194/bg-12-2753-2015, 2015.

Lehmann, A., Myrberg, K., and Höflich, K.: A statistical approach to coastal upwelling in the Baltic Sea based on the analysis of satellite data for 1990–2009, Oceanologia, 54, 369–393, https://doi.org/10.5697/oc.54-3.369, 2012.

https://doi.org/10.5194/egusphere-2026-3945
Preprint. Discussion started: 14 July 2026

Lenschow, D. H., Wulfmeyer, V., and Senff, C.: Measuring second- through fourth-order moments in noisy data, Journal of Atmospheric and Ocean Technology, 17, 1330–1347, https://doi.org/10.1175/1520-0426(2000)017<1330:MSTFOM>2.0.CO;2, 2000.

Lips, I., Rünk, N., Kikas, V., Meerits, A., and Lips, U.: High-resolution dynamics of the spring bloom in the Gulf of Finland of the Baltic Sea, Journal of Marine Systems, 129, 135–149, https://doi.org/10.1016/j.jmarsys.2013.06.002, 2014.

Löffler, A., Schneider, B., Perttilä, M., and Rehder, G.: Air–sea CO_2 exchange in the Gulf of Bothnia, Baltic Sea, Continental Shelf Research, 37, 46–56, https://doi.org/10.1016/j.csr.2012.02.002, 2012.

Macreadie, P. I., Costa, M. D. P., Atwood, T. B., Friess, D. A., Kelleway, J. J., Kennedy, H., Lovelock, C. E., Serrano, O., and Duarte, C. M.: Blue carbon as a natural climate solution, Nature Reviews Earth & Environment, 2, 826–839, https://doi.org/10.1038/s43017-021-00224-1, 2021.

Mahabbati, A., Beringer, J., Leopold, M., McHugh, I., Cleverly, J., Isaac, P., and Izady, A.: A comparison of gap-filling algorithms for eddy covariance fluxes and their drivers, Geoscientific Instrumentation Methods and Data Systems, 10, 123–140, https://doi.org/10.5194/gi-10-123-2021, 2021.

Mahrt, L.: Flux sampling errors for aircraft and towers, Journal of Atmospheric and Ocean Technology, 15, 416–429, https://doi.org/10.1175/1520-0426(1998)015<0416:FSEFAA>2.0.CO;2, 1998.

Mammarella, I., Launiainen, S., Grönholm, T., Keronen, P., Pumpanen, J., Rannik, U., and Vesala, T.: Relative humidity effect on the high-frequency attenuation of water vapor flux measured by a closed-path eddy covariance system, Journal of Atmospheric and Ocean Technology, 26, 1856–1866, https://doi.org/10.1175/2009JTECHA1179.1, 2009.

Mammarella, I., Peltola, O., Nordbo, A., Järvi, L., and Rannik, Ü.: Quantifying the uncertainty of eddy covariance fluxes due to the use of different software packages and combinations of processing steps in two contrasting ecosystems, Atmos. Meas. Tech., 9, 4915–4933, https://doi.org/10.5194/amt-9-4915-2016, 2016.

Mammarella, I., Vähä, A., Kolari, P., Spence, K., Geilfus, N.-X., and Norkko, J.: ETC L2 ARCHIVE from Tvärminne, 2022–2024, https://hdl.handle.net/11676/dYgjm6ghFvsiV5-PyrhOiSJn, 2025.

Mauder, M., Cuntz, M., Drüe, C., Graf, A., Rebmann, C., Schmid, H. P., Schmidt, M., and Steinbrecher, R.: A strategy for quality and uncertainty assessment of long-term eddy-covariance measurements, Agricultural and Forest Meteorology, 169, 122–135, https://doi.org/https://doi.org/10.1016/j.agrformet.2012.09.006, 2013.

Meier, H. E. M., Kniebusch, M., Dieterich, C., Gröger, M., Zorita, E., Elmgren, R., Myrberg, K., Ahola, M. P., Bartosova, A., Bonsdorff, E., Börgel, F., Capell, R., Carlén, I., Carlund, T., Carstensen, J., Christensen, O. B., Dierschke, V., Frauen, C., Frederiksen, M., Gaget, E., Galatius, A., Haapala, J. J., Halkka, A., Hugelius, G., Hünicke, B., Jaagus, J., Jüssi, M., Käyhko, J., Kirchner, N., Kjellström, E., Kulinski, K., Lehmann, A., Lindström, G., May, W., Miller, P. A., Mohrholz, V., Müller-Karulis, B., Pavón-Jordán, D., Quante, M., Reckermann, M., Rutgersson, A., Savchuk, O. P., Stendel, M., Tuomi, L., Viitasalo, M., Weisse, R., and Zhang, W.: Climate change in the Baltic Sea region: a summary, Earth System Dynamics, 13, 457–593, https://doi.org/10.5194/esd-13-457-2022, 2022.

Merkouriadi, I. and Leppäranta, M.: Long-term analysis of hydrography and sea-ice data in Tvärminne, Gulf of Finland, Baltic Sea, Climate Change, 124, 849–859, https://doi.org/10.1007/s10584-014-1130-3, 2014.

Neumann, T., Eilola, K., Gustafsson, B., Muller-Karulis, B., Kuznetsov, I., Meier, H. E. M., and Savchuk, O. P.: Extremes of temperature, oxygen and blooms in the Baltic Sea in a changing climate, AMBIO, 41, 574–585, https://doi.org/10.1007/s13280-012-0321-2, 2012.

Norman, M., Parampil, S. R., Rutgersson, A., and Sahlée, E.: Influence of coastal upwelling on the air–sea gas exchange of CO_2 in a Baltic Sea basin, Tellus Series B: Chemical and Physical Meteorology, 65, https://doi.org/10.3402/tellusb.v65i0.21831, 2013a.

https://doi.org/10.5194/egusphere-2026-3945
Preprint. Discussion started: 14 July 2026

Norman, M., Rutgersson, A., and Sahlée, E.: Impact of improved air–sea gas transfer velocity on fluxes and water chemistry in a Baltic Sea model, Journal of Marine Systems, 111, 175–188, https://doi.org/10.1016/j.jmarsys.2012.10.013, 2013b.

Ohlson, M. and Anderson, L.: Recent investigation of total carbonate in the Baltic Sea – Changes from the past as a result of acid-rain, Marine Chemistry, 30, 259–267, https://doi.org/10.1016/0304-4203(90)90075-N, congress of the International Union of Pure and Applied Chemistry: Atmospheric and Marine Chemistry, Stockholm, Sweden, Aug 02–07, 1989, 1990.

Probst, P., Wright, M. N., and Boulesteix, A.-L.: Hyperparameters and tuning strategies for random forest, Wiley Interdisciplinary Reviews: Data Mining and Knowledge Discovery, 9, https://doi.org/10.1002/widm.1301, 2019.

Rannik, Ü., Peltola, O., and Mammarella, I.: Random uncertainties of flux measurements by the eddy covariance technique, Atmos. Meas. Tech., 9, 5163–5181, https://doi.org/10.5194/amt-9-5163-2016, 2016.

Regnier, P., Resplandy, L., Najjar, R. G., and Ciais, P.: The land-to-ocean loops of the global carbon cycle, Nature, 603, 401–410, https://doi.org/10.1038/s41586-021-04339-9, 2022.

Richardson, A. D. and Hollinger, D. Y.: A method to estimate the additional uncertainty in gap-filled NEE resulting from long gaps in the CO_2 flux record, Agricultural and Forest Meteorology, 147, 199–208, https://doi.org/10.1016/j.agrformet.2007.06.004, 2007.

Rohlfer, E. K., Villnäs, A., Gustafsson, C., Gammal, J., Kauppi, L., Attard, K., Norkko, J., and Norkko, A.: Carbon cycling across coastal soft sediments: the contribution of macrofaunal communities to seafloor respiration, Marine Environmental Research, 215, 107 812, https://doi.org/10.1016/j.marenvres.2025.107812, 2026.

Roth, F., Broman, E., Sun, X., Bonaglia, S., Nascimento, F., Prytherch, J., Brüchert, V., Lundevall Zara, M., Brunberg, M., Geibel, M. C., Humborg, C., and Norkko, A.: Methane emissions offset atmospheric carbon dioxide uptake in coastal macroalgae, mixed vegetation and sediment ecosystems, Nature Communications, 14, https://doi.org/10.1038/s41467-022-35673-9, 2023.

Rutgersson, A., Norman, M., Schneider, B., Pettersson, H., and Sahlée, E.: The annual cycle of carbon dioxide and parameters influencing the air–sea carbon exchange in the Baltic Proper, Journal of Marine Systems, 74, 381–394, https://doi.org/10.1016/j.jmarsys.2008.02.005, 2008.

Rutgersson, A., Pettersson, H., Nilsson, E., Bergström, H., Wallin, M. B., Nilsson, E. D., Sahlée, E., Wu, L., and Mårtensson, E. M.: Using land-based stations for air–sea interaction studies, Tellus A: Dynamic Meteorology and Oceanography, 72, https://doi.org/10.1080/16000870.2019.1697601, 2020.

Schneider, B., Gülzow, W., Sadkowiak, B., and Rehder, G.: Detecting sinks and sources of CO_2 and CH_4 by ferrybox-based measurements in the Baltic Sea: Three case studies, Journal of Marine Systems, 140, 13–25, https://doi.org/10.1016/j.jmarsys.2014.03.014, 2014.

Stekhoven, D. J. and Bühlmann, P.: MissForest—non-parametric missing value imputation for mixed-type data, Bioinformatics, 28, 112–118, https://doi.org/10.1093/bioinformatics/btr597, 2012.

Stockmayer, V. and Lehmann, A.: Variations of temperature, salinity and oxygen of the Baltic Sea for the period 1950 to 2020, Oceanologia, 65, 466–483, https://doi.org/10.1016/j.oceano.2023.02.002, 2023.

Thakur, R. C., Peltola, M., Spence, K., Vähä, A., Haapanala, S., Ke, P., Ezhova, E., Hellén, H., Geilfus, N.-X., Chan, T., Norkko, J., Mammarella, I., Ehn, M., Norkko, A., and Kulmala, M.: Coastal-SMEAR – introduction to infrastructure and capacity of the atmospheric observatory in Tvärminne, Finland, Boreal Environment Research, 30, 195–219, https://doi.org/10.60910/ber2025.7rkh-0d75, 2025.

Thomas, H. and Schneider, B.: The seasonal cycle of carbon dioxide in Baltic Sea surface waters, Journal of Marine Systems, 22, 53–67, https://doi.org/10.1016/S0924-7963(99)00030-5, 1999.

Tokoro, T., Watanabe, K., Tada, K., and Kuwae, T.: Air–water CO_2 flux in shallow coastal waters: Theory, methods, and empirical studies, in: Blue carbon in shallow coastal ecosystems, pp. 153–184, Springer, Singapore, 2019.

https://doi.org/10.5194/egusphere-2026-3945
Preprint. Discussion started: 14 July 2026

Upstill-Goddard, R. C.: Air–sea gas exchange in the coastal zone, Estuarine, Coastal and Shelf Science, 70, 388–404, https://doi.org/10.1016/j.ecss.2006.05.043, 2006.

Uth, C., Asmala, E., and Lewandowska, A. M.: Phytoplankton community composition as a driver of annual autochthonous organic carbon dynamics in the northern coastal Baltic Sea, Marine Ecological Progress Series, 745, 13–24, https://doi.org/10.3354/meps14685, 2024.

Vähä, A., Jansen, J., Spence, K., Norkko, J., Norkko, A., and Mammarella, I.: Eddy covariance, meteorological and oceanographical data from Tvärminne, Finland during 2022–2024 (Version v1) [Data set], https://doi.org/10.5281/zenodo.21135816, 2026.

Wesslander, K., Omstedt, A., and Schneider, B.: Inter-annual and seasonal variations in the air–sea CO_2 balance in the central Baltic Sea and the Kattegat, Continental Shelf Research, 30, 1511–1521, https://doi.org/10.1016/j.csr.2010.05.014, 2010.

Wesslander, K., Hall, P., Hjalmarsson, S., Lefevre, D., Omstedt, A., Rutgersson, A., Sahlee, E., and Tengberg, A.: Observed carbon dioxide and oxygen dynamics in a Baltic Sea coastal region, Journal of Marine Systems, 86, 1–9, https://doi.org/10.1016/j.jmarsys.2011.01.001, 2011.

Wright, M. N. and Ziegler, A.: ranger: A fast implementation of random forests for high dimensional data in C++ and R, Journal of Statistical Software, 77, 1–17, https://doi.org/10.18637/jss.v077.i01, 2017.

Zhang, S., Wu, L., Arnqvist, J., Hallgren, C., and Rutgersson, A.: Mapping coastal upwelling in the Baltic Sea from 2002 to 2020 using remote sensing data, International Journal of Applied Earth Observation and Geoinformation, 114, https://doi.org/10.1016/j.jag.2022.103061, 2022.